IEEE Access
Multidisciplinary ⁝ Rapid Review ⁝ Open Access Journal

Received 15 July 2026, accepted 13 August 2026, date of publication 20 August 2026, date of current version 3 September 2026.

Digital Object Identifier 10.1109/ACCESS.2026.3725272

RESEARCH ARTICLE

A Low-Profile Hybrid Decoupling Method for Ultra-Compact Planar Antenna Arrays

SINA HASIBI TAHERI[1], ALI LALBAKHSH[2], (Senior Member, IEEE), NABEEL ZAHUR[1], SLAWOMIR KOZIEL[3,4], (Fellow, IEEE), STANISLAW SZCZEPANSKI[4], (Member, IEEE), AND AMIRHASSAN ZAREANBORJI[2], (Member, IEEE)

[1]School of Engineering, Macquarie University, Sydney, NSW, Australia
[2]UNSW College, Sydney, NSW, Australia
[3]Department of Engineering, Engineering Optimization and Modeling Center, Reykjavik University, 102 Reykjavik, Iceland
[4]Faculty of Electronics, Telecommunications and Informatics, Gdańsk University of Technology, 80-233 Gdańsk, Poland

Corresponding author: Sina Hasibi Taheri (sina.hasibitaheri@mq.edu.au)

This work was supported in part by the Macquarie University International Research Stipend Program (RTP) Scholarship funded by the Commonwealth Government, Australia; in part by Icelandic Research Fund under Grant 2410297; and in part by the National Science Centre of Poland under Grant 2022/47/B/ST7/00072.

ABSTRACT This paper presents a novel and compact decoupling methodology for ultra-compact planar antenna arrays with center-to-center spacing smaller than 0.3λ. In such densely packed configurations, strong multidirectional mutual coupling significantly degrades the array performance. To address this challenge, a comprehensive decoupling strategy is proposed for a 2 × 2 array operating in the 5.8–6 GHz band. The approach integrates three coordinated mechanisms: I-shaped metallic strips for coupling-path cancellation, a dumbbell-shaped defected ground structure (DGS) for ground-current suppression, and dielectric perturbation for reducing substrate-mediated coupling. The proposed structure achieves effective two-dimensional decoupling while maintaining a low-profile and easy-to-fabricate configuration. By performing a systematic parametric study and Genetic Algorithm (GA) the structure is optimized in the multidimensional design space. Both simulated and measured results demonstrate that the proposed method successfully reduces the transmission coefficients between array elements to below −20 dB across the target frequency band, satisfying the critical design requirement. The achieved isolation enhancement does not degrade the impedance matching, and the measured radiation patterns further demonstrate that the proposed decoupling structure improves the realized gain by 2.85 dB and 4.34 dB at the lower and upper edges of the operating frequency band, respectively.

INDEX TERMS Ultra-compact arrays, decoupling structures, mutual coupling reduction, isolation.

I. INTRODUCTION

The growing demand for high-capacity wireless communication systems has accelerated the deployment of compact antenna arrays in applications such as 5G base stations [1], MIMO terminals [2], [3], [4], and broadband sensing platforms [5]. To satisfy size, profile, and integration requirements, antenna elements are often placed with reduced inter-element spacing, which intensifies electromagnetic interaction between neighboring radiators and leads to strong mutual coupling [6]. As the spacing decreases, mutual coupling degrades impedance matching, port isolation, radiation characteristics, and realized gain, while also deteriorating polarization purity and axial-ratio bandwidth in polarized arrays [7], [8]. In phased array and MIMO systems, these effects further limit beam-scanning capability and channel capacity, making coupling suppression a critical challenge in compact array design [9], [10].

To mitigate mutual coupling, several decoupling approaches have been reported in the literature. Circuit-based techniques, including neutralization lines [11], [12], [13], decoupling networks [14], [15], and tailored excitation methods [16],

The associate editor coordinating the review of this manuscript and approving it for publication was Yunlong Cai.

[17] introduce compensating currents to cancel coupling paths. Although capable of providing high isolation, these methods are often narrowband, sensitive to fabrication tolerances, and difficult to scale for compact or broadband arrays.

Parasitic metallic structures [12], [18], [19], [20], including metal walls, strips, and side-loaded conductors, have also been widely employed to improve isolation through destructive interference of coupling fields. Side-loaded metal [21] and parasitic monopole-like structures [22] provide attractive fabrication simplicity and compact implementation. Nevertheless, their performance generally depends on precise geometrical tuning and often remains effective only over limited frequency ranges. More importantly, planar arrays exhibit multiple coupling mechanisms between horizontal, vertical, and diagonal element pairs, making it difficult for a single parasitic element to suppress all dominant coupling paths simultaneously.

Electromagnetic structure-based techniques, including electromagnetic bandgap (EBG) [23], [24], [25], defected ground structures (DGS) [26], [27], [28], frequency-selective surfaces (FSS) [29], [30], [31], [32], and metasurface-based layers [33], [34], [35], [36], suppress coupling by modifying surface-wave propagation and near-field interactions. More recently, hybrid decoupling strategies combining multiple physical mechanisms have been explored [37], [38]. By integrating reflective, parasitic, or resonant structures, hybrid approaches can simultaneously suppress multiple coupling components and achieve improved isolation bandwidth.

Despite these advances, many reported techniques rely on multilayer implementations, increased structural complexity, or additional profile height, limiting their applicability in ultra-compact and low-profile arrays. Furthermore, achieving effective coupling suppression in densely packed planar arrays remains particularly challenging due to the multidirectional nature of the coupling mechanisms.

Motivated by the stringent requirements of ultra-compact array configurations, this work presents the design and experimental validation of a 2 × 2 antenna array with center-to-center spacing smaller than 0.3λ, where multidirectional mutual coupling becomes inherently severe. Unlike conventional techniques that primarily target coupling suppression along a single direction or under moderate spacing conditions, the proposed approach simultaneously mitigates coupling in both principal planar directions. The employed upper structure does not operate as a conventional metasurface for phase correction or direct gain enhancement, instead, it functions as a hybrid decoupling mechanism, where gain improvement is achieved indirectly through mutual coupling suppression and enhanced radiation efficiency. Particular emphasis is placed on preserving realized gain and radiation integrity while maintaining a low-profile and fabrication-friendly structure without relying on complex multilayer assemblies or intricate feeding networks.

The main contributions of this work are summarized as follows:

- A hybrid decoupling methodology is proposed for ultra-compact planar antenna arrays with center-to-center spacing smaller than 0.3λ, where strong multidirectional coupling mechanisms dominate.
- The proposed structure integrates I-shaped metallic strips, a dumbbell-shaped DGS, and dielectric perturbation into a unified framework, enabling simultaneous coupling suppression without relying on conventional λ/4 spacing or multilayer metasurfaces.
- The optimized design achieves isolation better than −20 dB within the 5.8–6 GHz band while preserving impedance matching and realized gain, demonstrating effective coupling suppression without radiation-performance degradation.
- The proposed decoupling structure maintains a simple, low-profile, and fabrication-friendly configuration, providing a scalable and practical solution for next-generation ultra-compact antenna arrays.

This work is organized as follows. Section II details the antenna design procedure and provides the comprehensive analysis of the structure. Section III provides the simulation and measurement results of the designed structure and finally, Section IV presents the conclusions of the study.

II. ANTENNA DESIGN AND ANALYSIS

The overall configuration of the proposed hybrid decoupling antenna array is illustrated in Fig. 1. The antenna consists of a 2 × 2 planar probe-fed patch array operating at 5.8 GHz, a passive decoupling layer composed of I-shaped resonant strips, a dumbbell-shaped DGS, and localized dielectric perturbations introduced in both the antenna and decoupling substrates. The radiating elements are excited using a conventional coaxial probe-fed configuration, and the center-to-center spacing between adjacent elements is intentionally reduced to less than 0.3λ, creating a strongly coupled electromagnetic environment in which multidirectional mutual coupling becomes a dominant design challenge. These components collectively realize the proposed hybrid decoupling mechanism, enabling simultaneous suppression of the dominant coupling paths while maintaining a compact and low-profile configuration. To clearly illustrate the contribution of each decoupling mechanism, the proposed antenna is developed and analyzed in a systematic step-by-step manner. The following subsections begin with the reference antenna array and progressively introduce each decoupling technique until the final optimized configuration is achieved.

A. CONFIGURATION OF THE 2 × 2 MICROSTRIP ARRAY

The configuration of the proposed ultra-compact 2 × 2 antenna array is shown in Fig. 2. The array consists of four identical coaxial probe-fed radiating elements arranged

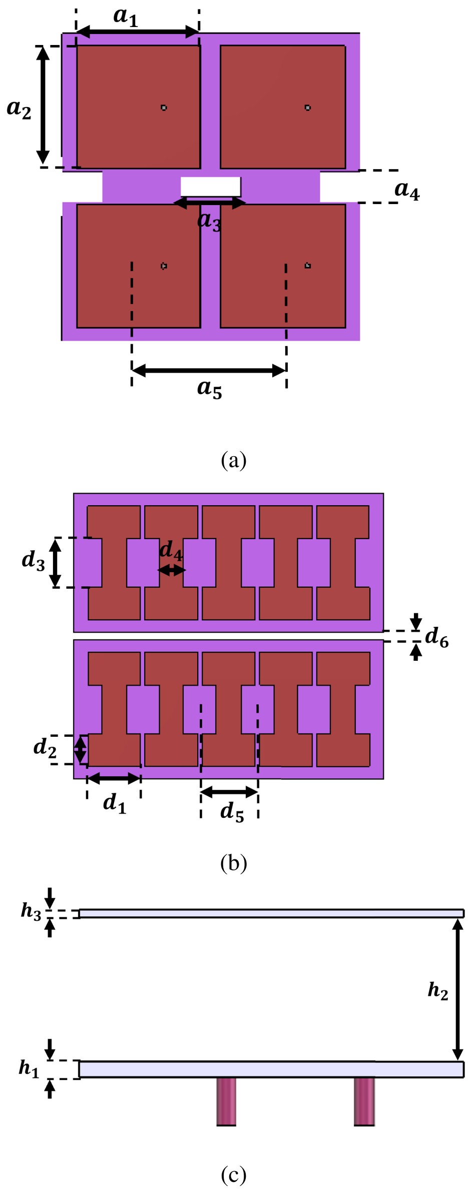

FIGURE 1. Top view of the (a) array, (b) decoupling surface and (c) side view of the proposed structure with corresponding parameters.

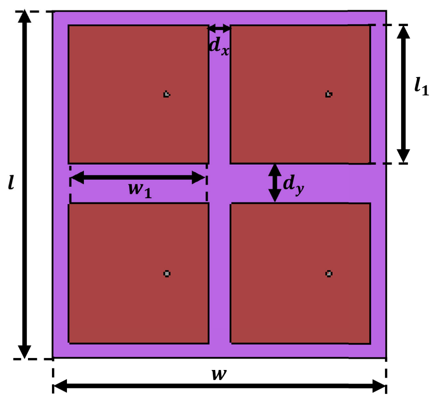

FIGURE 2. Geometry of the proposed 2 × 2 ultra-compact antenna array.

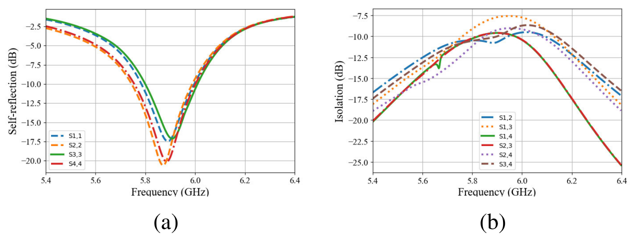

FIGURE 3. (a) Reflection and (b) isolation results of the 2 × 2 microstrip array.

in a planar square topology. The operating frequency is 5.8 GHz.

Each radiating element is implemented on a Rogers 4350B laminate with relative permittivity $\varepsilon_r = 3.66$ and loss tangent $\tan\delta = 0.0037$, and substrate thickness $h = 1.52$ mm. The planar radiator has dimensions $L \times W$, where L and W denote the effective length and width of the patch, respectively. The coaxial feed probe is located at an optimized position (x_f, y_f) from the patch center to achieve impedance matching at 5.8 GHz.

The four elements are symmetrically positioned along both the x- and y-directions with a center-to-center spacing of $d_{x,y} = 2$ mm, corresponding to $d = 0.28\lambda_0$ at 5.8 GHz. This extremely compact spacing intentionally places the array in a strong mutual coupling regime representative of densely packed MIMO systems. Under such tight separation, pronounced near-field interaction and surface-wave coupling occur simultaneously in both principal directions of the planar array.

Owing to the severe electromagnetic interaction introduced by the sub-$0.3\lambda_0$ spacing, the baseline array configuration is first established without any decoupling structure. This reference configuration enables systematic analysis of mutual coupling mechanisms and radiation performance degradation before the progressive introduction of coupling mitigation techniques in subsequent subsections. Fig.3 illustrates the simulated reflection coefficient ($S_{i,i}$) and isolation terms ($S_{i,j}$) for the compact 2 × 2 array. As indicated in Fig.3-b, strong coupling exists between different radiating elements in the desired frequency range.

Another way of showing the coupling between the array's elements is using the E-field distribution of the radiating elements. As indicated from Fig.4, at 5.8 GHz strong coupling exists between adjacent elements.

B. ROW-WISE METASURFACE DECOUPLING STRATEGY

As observed in Fig. 4, from the baseline 2 × 2 array configuration, the dominant mutual coupling occurs between adjacent elements within each row due to the ultra-compact center-to-center spacing ($d < 0.3\lambda_0$). At 5.8 GHz, the strong electric near-field interaction and surface-wave propagation along the row direction lead to significant energy transfer between neighboring elements.

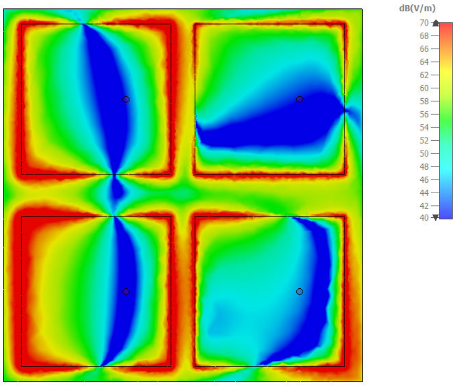

FIGURE 4. E-field distribution over 2 × 2 array at 5.8 GHz.

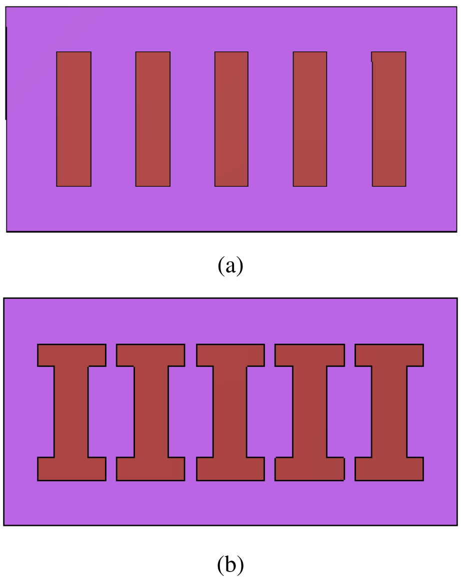

FIGURE 5. Top view of the (a) Vertical strips and (b) I-shaped patch.

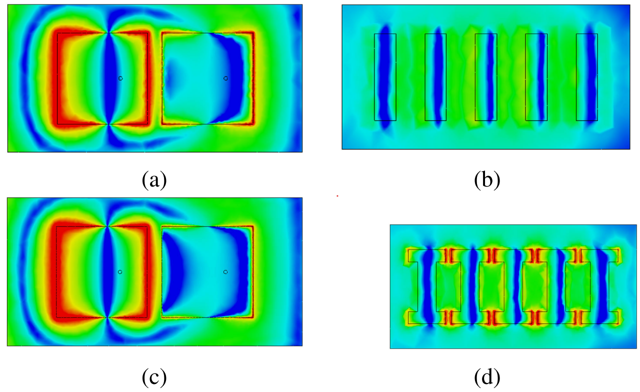

FIGURE 6. E-field distribution of the (a) one row of the patch array loaded with the vertical strips, (b) vertical strips, (c) one row of the patch array loaded with I-shaped patches and (d) I-shaped patches.

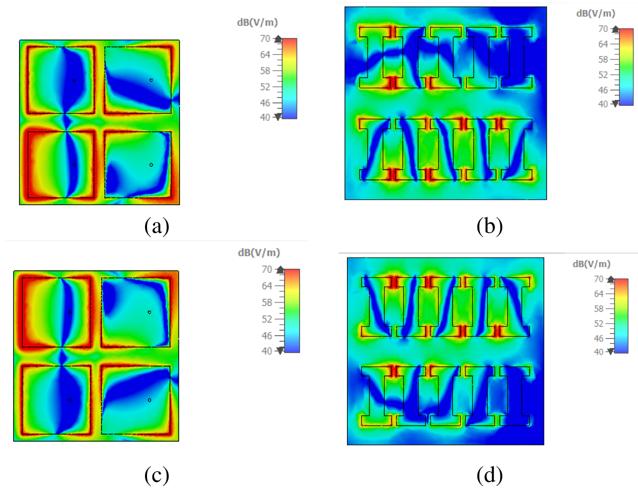

FIGURE 7. E-field distribution of 2 × 2 array loaded with two rows of I-shape element over the (a) array and (b) decoupling surface when port 1 (bottom left) is excited,and over (c) array and (d) decoupling surface when port 3 (top left) is excited.

To mitigate this dominant coupling mechanism, using printed vertical strips, as indicated in Fig. 5a, has been suggested above each row of antennas [39], [40]. The metasurface is positioned and designed to primarily influence the electromagnetic field distribution along the row direction, where the strongest coupling occurs. By tailoring the unit-cell geometry and its periodic arrangement, the metasurface modifies the electric field distribution near the antennas. However, employing only the conventional vertical strip above the antenna array does not provide sufficient mutual coupling reduction in ultra-compact configurations. In order to enhance the decoupling capability of the structure, two horizontal metallic extensions are introduced at the ends of the vertical strip, forming an I-shaped patch as shown in Fig. 5b.

Fig. 6 illustrates the electric field distributions for both the simple vertical strip and the proposed I-shaped configuration, placed above one row of the patch array. It can be observed that the I-shaped element exhibits stronger electromagnetic interaction within the decoupling structure while simultaneously reducing the electric field intensity in the region between the two radiating patches. The enhanced field confinement around the I-shaped element, together with the suppressed field strength between adjacent antennas, clearly indicates improved decoupling performance compared to the traditional vertical strip design.

It is important to emphasize that the metasurface is intentionally applied in a row-wise manner rather than as a full-array superstrate. This targeted implementation enables effective decoupling between adjacent elements in each row while maintaining structural simplicity and low profile. Consequently, two identical metasurface sections are employed, one for each row of the 2 × 2 array, to independently suppress intra-row mutual coupling.

However, although the row-wise metasurface significantly reduces coupling between elements along the horizontal direction, residual strong mutual interaction remains between the two rows as depicted in Fig. 7.

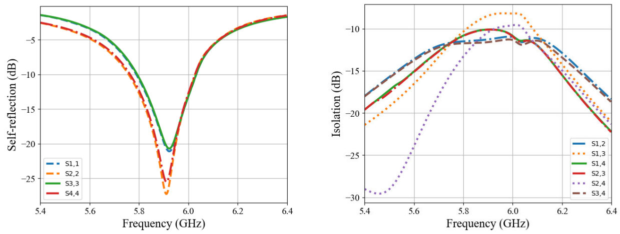

(a) (b)

FIGURE 8. (a) Reflection and (b) isolation results of the 2 × 2 microstrip array with the addition of two rows of I-shaped patches.

As indicted in Fig.7, the decoupling surface performance deteriorates by adding another row to the structure which can be related to the strong inter-row coupling. This inter-row coupling originates from vertical near-field interaction and space-wave coupling mechanisms that are not fully mitigated by the directional metasurface configuration. These effects can also be observed in the simulated s-parameters results, as shown in Fig.8. As observed in Fig. 8-b, the isolation within each row is noticeably improved compared to that shown in Fig. 3-b. However, significant mutual coupling still persists between the two rows. The following section therefore focuses on analyzing the underlying mechanisms of this remaining inter-row coupling and presents an effective strategy for its suppression.

C. APPLYING DGS

To further decrease the mutual coupling, especially the existing coupling between the rows, a DGS structure is introduced. A DGS modifies the current distribution on the ground plane by etching specific geometrical defects, thereby altering its effective inductive–capacitive behavior. From an electromagnetic perspective, the presence of a DGS increases the equivalent impedance of the ground plane along selected directions, effectively interrupting surface current flow and suppressing surface-wave propagation between antenna elements. This could be beneficial in ultra-compact arrays, where ground-plane currents contribute significantly to mutual coupling. As shown in Fig. 9, the DGS is a simple strip that is cut from the ground plane. The simulated results of the S-parameter of the array with the addition of the DGS structure are shown in Fig.9. As indicated in Fig.10-a, addition of the DGS slightly degrades the reflection coefficient performance but improves the inter-row mutual coupling performance, such as $S_{31}, S_{41}, \ldots$, as shown in Fig. 10-b.

Moreover, considering the distribution of the E-field in the array, reported in Figs.11-(a) and (b), with the DGS and I-shaped patch on the top reiterates the improvement in the isolation between the elements in the array compared to the previous configurations.

To further suppress mutual coupling between the vertically adjacent element pairs (1,3) and (2,4), while simultaneously improving the impedance matching of each antenna

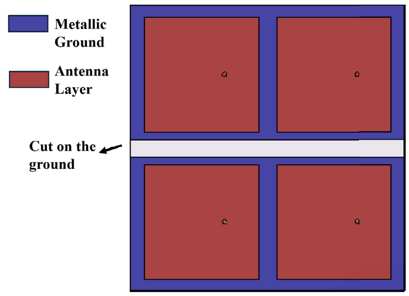

FIGURE 9. Top view of the cut on the ground layer of the microstrip patch array.

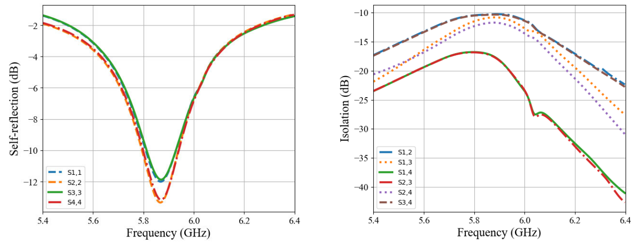

(a) (b)

FIGURE 10. (a) Reflection and (b) isolation results of the loaded 2 × 2 microstrip array with the addition of DGS.

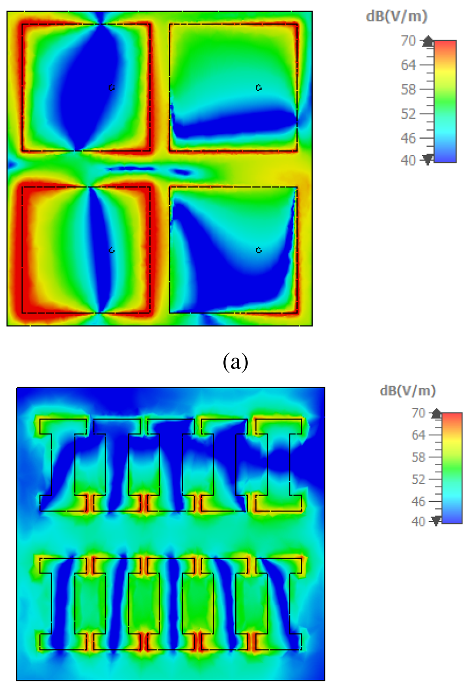

(a)

(b)

FIGURE 11. E-field distribution of the configuration over the (a) array and (b) decoupling surface with the addition of DGS at 5.8 GHz.

element, a modification to the existing DGS is proposed. Specifically, a pair of stubs is introduced at the ends of the current ground defect, forming a dumbbell-shaped

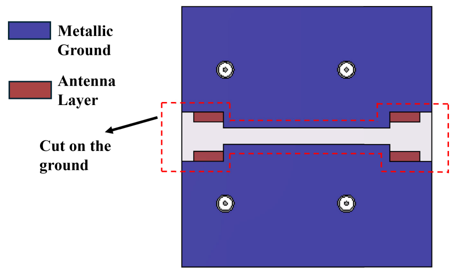

FIGURE 12. Bottom view of the dumbell-shaped DGS on the ground layer of the microstrip patch array.

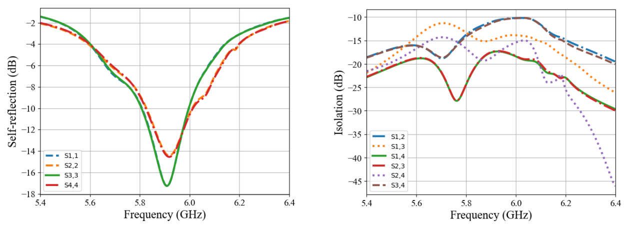

(a) (b)

FIGURE 13. (a) Reflection and (b) isolation results of the loaded 2 × 2 microstrip array with the addition of dumbell-shaped DGS.

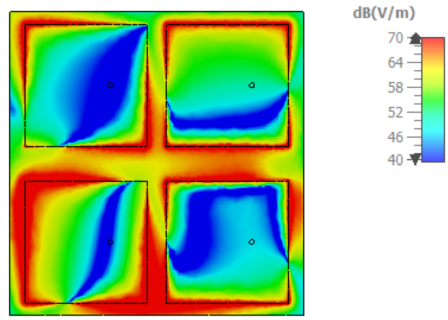

(a)

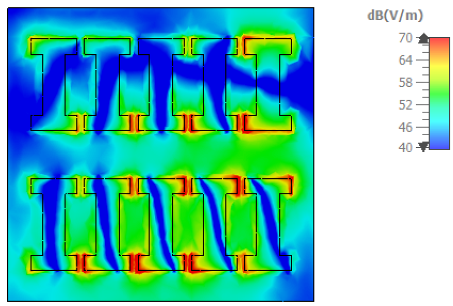

(b)

FIGURE 14. E-field distribution of the configuration over the (a) array and (b) decoupling surface with dumbell-shaped DGS at 5.8 GHz.

DGS configuration, as illustrated in Fig. 12. This geometry enhances the perturbation of ground-plane current distribution and increases the effective impedance along the inter-row direction, thereby providing stronger coupling suppression and improved matching performance.

To conclude, the dumbbell-shaped DGS is selected due to its simple geometry and effective capability in suppressing surface-wave propagation and perturbing ground current distribution. The introduced slot modifies the equivalent inductive and capacitive characteristics of the ground plane, thereby reducing coupling between adjacent antenna elements. Moreover, the dumbbell-shaped DGS is a well-established and widely employed topology in microwave and antenna engineering due to its compact resonant behavior, fabrication simplicity, and effective suppression of undesired electromagnetic propagation. Previous studies have successfully utilized dumbbell-shaped DGS structures in filters, transmission lines, and antenna systems to improve isolation and electromagnetic performance [41], [42]. These characteristics make it particularly suitable for compact antenna decoupling applications.

Simulated results of the S-parameters, shown in Fig.13 and Fig.14, and the distribution of the electric field near the antennas shows that the addition of stubs and form the dumbell-shaped DGS effectively decrease the mutual coupling for the vertical adjacent antennas and also improve the matching condition of each element.

D. LOCALIZED DIELECTRIC PERTURBATION

Although the incorporation of the dumbbell-shaped DGS significantly improves the inter-row isolation, residual coupling persists due to the strong near-field interaction within the dielectric medium. In ultra-compact arrays, a considerable portion of the mutual coupling energy is confined within the substrate, where the dielectric supports intense electric-field concentration and surface-wave propagation. This dielectric confinement enhances capacitive coupling between adjacent elements and facilitates the transfer of electromagnetic energy through both the antenna substrate and the superimposed decoupling structure. Therefore, to further suppress these substrate-mediated coupling paths, a localized dielectric perturbation is introduced by selectively removing small portions of the dielectric substrate from both the antenna array and the proposed decoupling structure, as shown in Fig. 15. The resulting dielectric modification alters the local electromagnetic field distribution and provides an additional degree of freedom for reducing the remaining mutual coupling between adjacent elements. It should be emphasized that this localized dielectric perturbation is not intended to serve as a standalone or universal decoupling technique. Rather, it forms an integral part of the proposed hybrid decoupling methodology, complementing the I-shaped resonant strips and the dumbbell-shaped DGS to collectively achieve the desired isolation performance in the ultra-compact antenna array.

It is worth noting that the locations of the dielectric modification are selected based on the areas between the radiating elements with high levels of electromagnetic field distribution which can be seen in Fig.14. Here, by locally reducing the dielectric loading, the effective permittivity in

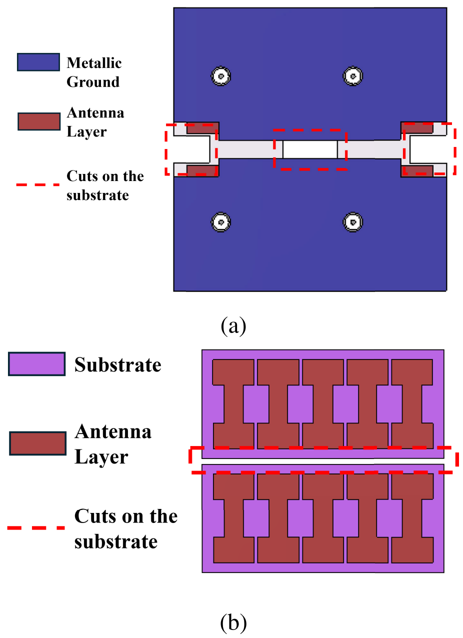

FIGURE 15. (a) Bottom view of the modified array and (b) Top view of the modified decoupling structure.

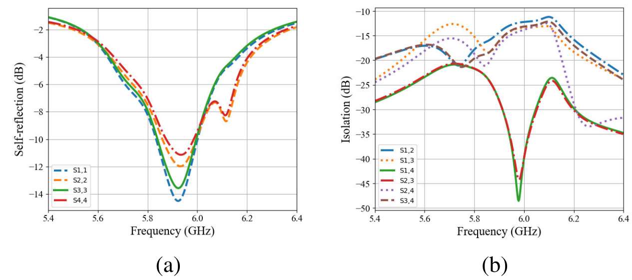

FIGURE 16. (a) Reflection and (b) isolation results of the loaded 2 × 2 microstrip array with the modification of the substrates in the structure.

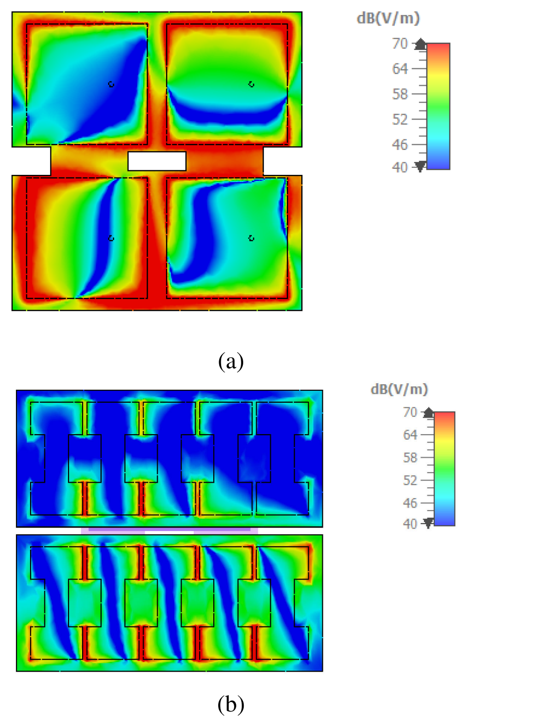

FIGURE 17. E-field distribution of the configuration over the (a) array and (b) decoupling surface with modified substrate structure at 5.8 GHz.

the coupling region is decreased, which weakens the stored electric energy and disrupts surface-wave propagation paths. From an electromagnetic standpoint, reducing the dielectric volume lowers the equivalent capacitive coupling between adjacent elements and increases radiation leakage into free space rather than confinement within the substrate. This effect is particularly beneficial in ultra-compact configurations, where strong near-field coupling dominates the overall interaction.

Moreover, applying the perturbation simultaneously to the array substrate and the decoupling layer ensures that both direct inter-element interaction and coupling caused by decoupling-structure are weakened. The reduction of dielectric confinement around the decoupling structure enhances its effectiveness by allowing stronger interaction with free-space fields while minimizing unintended energy storage within the dielectric medium.

The Simulation results, presented in Fig.16 and Fig.17, of the proposed modification on the array and decoupling substrate show the expected improvement in the isolation terms without sacrificing the impedance condition of each element.

It should be noted that the proposed localized dielectric perturbation is implemented through selective substrate removal in both the antenna and decoupling layers, which can be readily realized using conventional PCB fabrication techniques. Unlike extensive substrate removal, the proposed modification is highly localized, occupying only approximately 6% of the total substrate area and confined to the central region of the antenna structure, where its influence on the overall mechanical integrity is minimal. Furthermore, the substrate thickness is selected to provide sufficient mechanical rigidity, while dielectric spacers are employed to support the upper decoupling structure and maintain the required separation between the two layers throughout fabrication and measurement. Similar localized substrate modification techniques have been widely employed in antenna and microwave engineering to tailor electromagnetic field distributions and suppress undesired coupling mechanisms [43], [44], [45], [46]. Therefore, the proposed technique preserves fabrication simplicity while providing an additional degree of control over substrate-mediated coupling paths. The successful fabrication, assembly, and experimental characterization of the proposed prototype using conventional PCB technology further confirm the practical feasibility, mechanical robustness, and manufacturability of the proposed localized dielectric perturbation approach.

E. PARAMETRIC STUDY

Given the ultra-compact spacing and the multi-mechanism decoupling strategy employed in the proposed 2 × 2 array, a systematic parametric investigation is essential to fully understand the electromagnetic behavior of the structure. In such densely packed configurations, small variations in geometric parameters can significantly influence current distribution, field confinement, impedance matching, and mutual coupling characteristics. Therefore, evaluating the sensitivity of the proposed design to key structural parameters provides critical insight into the underlying decoupling mechanisms and ensures the robustness of the solution.

In particular, the dimensions associated with the decoupling elements, DGS, and the dielectric perturbation directly control the behavior of the system. These parameters determine the strength of ground-plane current interruption, the degree of electric-field redistribution, and the balance between isolation enhancement and radiation performance. Since coupling in the proposed ultra-compact array occurs simultaneously along two principal directions, parameter optimization must ensure effective suppression in both axes without introducing gain degradation or impedance mismatch. This subsection presents a detailed parametric study of the most influential design variables, highlighting their impact on isolation, impedance matching.

We begin by investigating the influence of the vertical stem length of the I-shaped strip, denoted as d_3. Varying the length of this central section modifies the effective electrical length of the decoupling element, thereby increasing its equivalent inductance and shifting its resonance toward lower frequencies. In this study, d_3 is varied from 3 mm to 7 mm to evaluate its impact on the coupling behavior. Since the I-shaped patch primarily affects the inter-row mutual coupling, the analysis focuses mainly on the transmission coefficient S_{21}.

As shown in Fig. 18-a, varying d_3 has a negligible effect on the reflection coefficient, indicating that the impedance matching of each antenna element remains largely unchanged. In contrast, Fig. 18-b demonstrates that d_3 significantly influences S_{21}, confirming that the vertical stem length plays a critical role in controlling the inter-row mutual coupling.

The second parameter under investigation is the length of the horizontal arm of the I-shaped strip, denoted as d_1. This parameter governs the electromagnetic interaction between adjacent I-shaped elements and is therefore expected to have a significant impact on the isolation performance. To evaluate its influence, d_1 is varied from 3 mm to 7 mm, and the corresponding reflection and transmission coefficients are shown in Fig. 19.

As observed in Fig. 19-a, varying d_1 has a negligible effect on the reflection coefficient, indicating that the impedance matching of the antenna elements remains stable. In contrast, Fig. 19-b demonstrates that d_1 significantly influences the isolation coefficient S_{21}. Notably, isolation is substantially improved for values of d_1 around 6 mm, confirming the strong role of the horizontal arms in enhancing the decoupling mechanism.

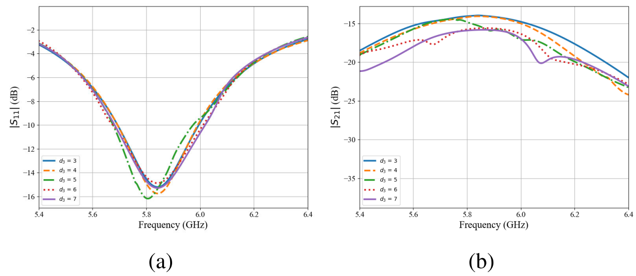

FIGURE 18. Parametric study of the vertical stem length d_3 of the I-shaped decoupling strip: (a) reflection coefficient S_{11} and (b) isolation coefficient S_{21}.

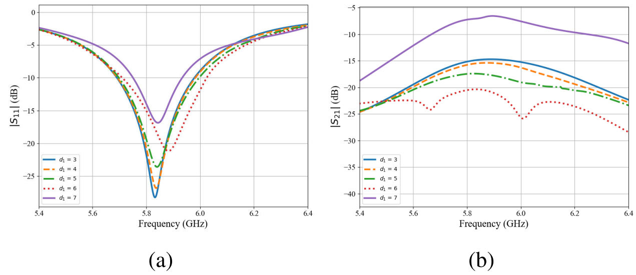

FIGURE 19. Parametric study of the horizontal arm length d_1 of the I-shaped decoupling strip: (a) reflection coefficient S_{11} and (b) isolation coefficient S_{21}.

It is worth emphasizing that when $d_1 = 3$ mm, the horizontal arms effectively vanish, reducing the I-shaped strip to a conventional vertical strip. The degraded isolation in this case clearly verifies the superior decoupling performance of the I-shaped configuration compared to a simple vertical strip. Furthermore, when $d_1 = 7$ mm, the horizontal arms of adjacent elements become electrically connected, altering the resonant behavior of the structure. In this condition, the decoupling element no longer operates as an effective resonator, which explains the observed deterioration in isolation performance.

The next parameter examined is the width of the horizontal arm of the I-shaped strip, denoted as d_2. This parameter influences the electromagnetic coupling between adjacent patches by modifying the effective current loop formed between neighboring decoupling elements. As d_2 increases, the effective loop area decreases, which reduces the equivalent inductance of the resonant structure and consequently shifts its resonance toward higher frequencies. To evaluate its influence, d_1 is varied from 1 mm to 5 mm, and the corresponding reflection and transmission coefficients are shown in Fig. 20.

This behavior is clearly observed in both Fig. 20-a and Fig. 20-b, where increasing d_2 results in a noticeable upward shift of the resonance frequency. The variation of d_2 has

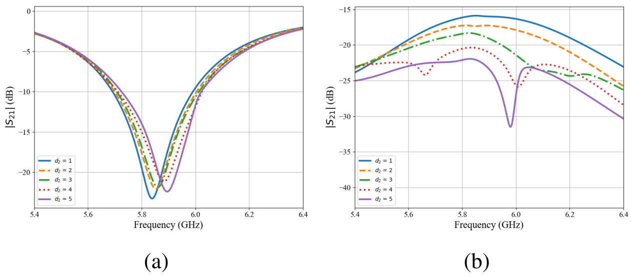

FIGURE 20. Effect of the horizontal arm width on the array performance: (a) reflection coefficient (b) transmission coefficient S_{21}.

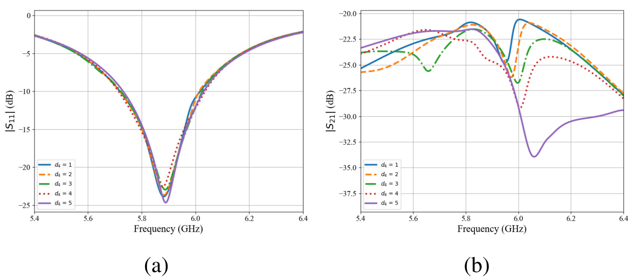

FIGURE 21. Effect of the width of vertical strip on the array performance: (a) reflection coefficient (b) transmission coefficient.

minimal impact on the reflection coefficient, indicating that the impedance matching remains largely unaffected. However, it significantly influences the transmission coefficient S_{21}, demonstrating its strong role in controlling the isolation performance of the decoupling structure.

Another important geometric parameter of the I-shaped patch is the width of the vertical stem, denoted as d_4. This parameter exhibits a similar influence on the decoupling behavior as d_2, though with a comparatively weaker effect. As illustrated in Fig. 21, variations in d_4 lead to observable changes in the isolation performance while maintaining stable impedance characteristics.

Due to its moderate sensitivity, d_4 serves as an effective fine-tuning parameter in the final optimization stage of the decoupling structure, allowing precise adjustment of the resonance behavior to meet the targeted design specifications.

The final parameter investigated in the proposed structure is the length of the slot etched on the antenna substrate, denoted as a_3. This slot is introduced to suppress the mutual coupling between the rows by interrupting the ground-plane current distribution and reducing surface-wave propagation along the inter-row direction.

To evaluate its effect, a_3 is varied from 0 mm to 12 mm, and the corresponding transmission coefficient S_{31} (representing inter-row isolation) and reflection coefficient S_{11} are monitored. The simulated S-parameter results are presented in Fig. 22. It can be observed that increasing the slot length progressively reduces the mutual coupling, confirming the effectiveness of the substrate perturbation in suppressing inter-row interaction.

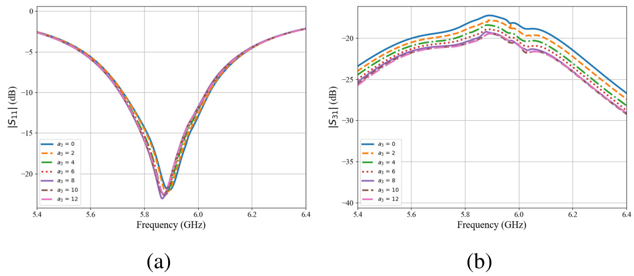

FIGURE 22. Study of the effect of the substrate slot length on the array performance: (a) reflection coefficient (b) transmission coefficient.

In particular, the comparison between $a_3 = 0$ mm (no slot) and the shortest nonzero slot clearly demonstrates the beneficial impact of introducing the substrate cut on the isolation performance. Meanwhile, the variation of a_3 produces no significant change in the reflection coefficient, indicating that the impedance matching of the antenna elements remains stable throughout the parametric range.

Another important design parameter is the vertical separation between the antenna array and the decoupling surface, which is treated as an independent optimization variable due to its strong influence on electromagnetic interaction, isolation performance, and overall antenna profile. In conventional decoupling or partially reflective surface configurations, the optimal spacing is typically close to $\lambda/4$, where constructive and destructive interference mechanisms can be effectively established. At approximately $\lambda/4$, the reflected fields from the decoupling surface can be properly phased to enhance radiation performance and improve isolation.

However, maintaining such a separation significantly increases the overall profile of the structure, which contradicts the objective of achieving an ultra-compact and low-profile array configuration. Therefore, in the proposed design, the separation distance is systematically optimized with the goal of minimizing the profile while preserving strong decoupling performance. By carefully adjusting this spacing, a balance is achieved between sufficient electromagnetic interaction with the decoupling surface and structural compactness. The final selected distance provides effective isolation enhancement without relying on the conventional $\lambda/4$ spacing, thereby maintaining the low-profile requirement of the proposed ultra-compact array.

III. FABRICATION, MEASUREMENT, AND PERFORMANCE VALIDATION

A. PROPOSED STRUCTURE AND DESIGN PARAMETERS

The final optimized configuration of the proposed ultra-compact 2 × 2 antenna array with the integrated decoupling structure is shown in Fig. 1. The array maintains a center-to-center spacing smaller than 0.3λ at the operating frequency, representing a highly compact planar arrangement.

The decoupling mechanism consists of three coordinated components: the I-shaped metallic strips placed above

TABLE 1. Optimized geometrical parameters of the proposed 2 × 2 array.

Parameter	Value (mm)
d_1	6
d_2	4
d_3	6
d_4	3
d_5	7
h_2	10
a_1	12.5
a_2	12.5
a_3	10
a_4	1.5
a_5	14.5

the array, the dumbbell-shaped DGS, and the dielectric perturbation applied to both the antenna substrate and the decoupling layer. These elements collectively suppress mutual coupling in both principal planar directions while preserving impedance matching and radiation performance.

The design objective was to achieve an isolation level better than −20 dB within the operating frequency range of 5.8–6 GHz. To systematically identify the optimal set of geometrical parameters that satisfies this requirement, a Genetic Algorithm (GA) optimization approach was employed. The GA is employed due to its robust global search capability and suitability for nonlinear electromagnetic optimization problems involving multiple strongly coupled design parameters. The proposed decoupling structure presents a multidimensional optimization space without an explicit analytical gradient, making GA an effective and computationally practical approach for identifying configurations satisfying the targeted isolation, matching, and radiation requirements. Although more recent optimization approaches, including machine learning- and artificial intelligence-assisted techniques, have attracted increasing interest, the primary objective of this work is to demonstrate the proposed hybrid decoupling methodology rather than compare optimization algorithms. The GA-based optimization enables efficient exploration of the multidimensional design space and facilitates convergence toward a configuration that simultaneously enhances isolation while preserving impedance matching and radiation performance. The optimized geometrical parameters of the proposed design are summarized in Table 1.

B. FABRICATION AND MEASUREMENT SETUP

To experimentally validate the proposed design, a prototype of the optimized 2 × 2 array was fabricated. Both the antenna layer and the decoupling structure were realized on Rogers RO4350B substrates with the thickness of 1.52 mm and 0.76 mm, respectively. Based on the parameters shown at 1, the overall size of the array with the loaded decoupling structure is $0.638\lambda_0 \times 0.638\lambda_0 \times 0.193\lambda_0$. A photograph of the fabricated prototype is presented in Fig. 23.

The S-parameters were measured using a calibrated vector network analyzer (VNA). Radiation characteristics, including realized gain and radiation patterns, were measured in an anechoic chamber under standard far-field conditions.

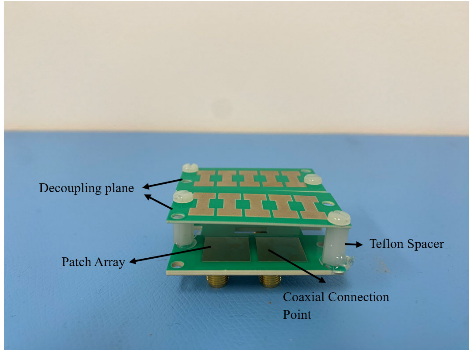

(a)

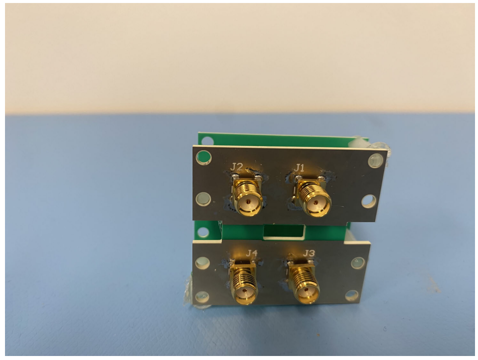

(b)

FIGURE 23. (a) Top and (b) back views of the fabricated prototype of the proposed array.

C. S-PARAMETER PERFORMANCE

Fig. 24 compares the simulated and measured S-parameters of the array with and without the proposed decoupling structure. Symmetric element pairs are omitted for brevity, as their responses are identical due to the structural symmetry of the array. According to Fig. 24-b, Without the decoupling structure, the ultra-compact spacing results in strong mutual coupling between adjacent elements. After incorporating the proposed decoupling mechanism, the transmission coefficient S_{21} is significantly reduced in both planar directions. The comparison between the results obtained before and after incorporating the proposed decoupling structure demonstrates that the transmission coefficients between the array elements are effectively reduced to below −20 dB. This confirms that the proposed decoupling mechanism successfully meets the targeted isolation requirement. Except for minor discrepancies between the simulated and measured results, which can be attributed to fabrication tolerances and slight shifts in the frequency response, the measured results show good agreement with the simulations, confirming the effectiveness of the proposed structure.

Moreover, as illustrated in Fig. 24-a, the reflection coefficient S_{11} remains stable after introducing the decoupling elements, indicating that the isolation enhancement does

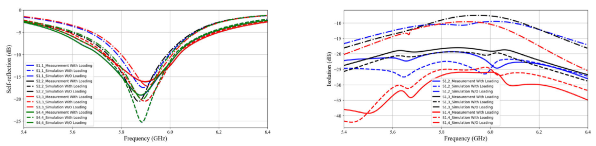

(a) (b)

FIGURE 24. **(a) Reflection and (b) isolation results of the measurement (solid line), simulation with the loading(dotted line) and simulation without the loading (dot and solid) of the proposed array.**

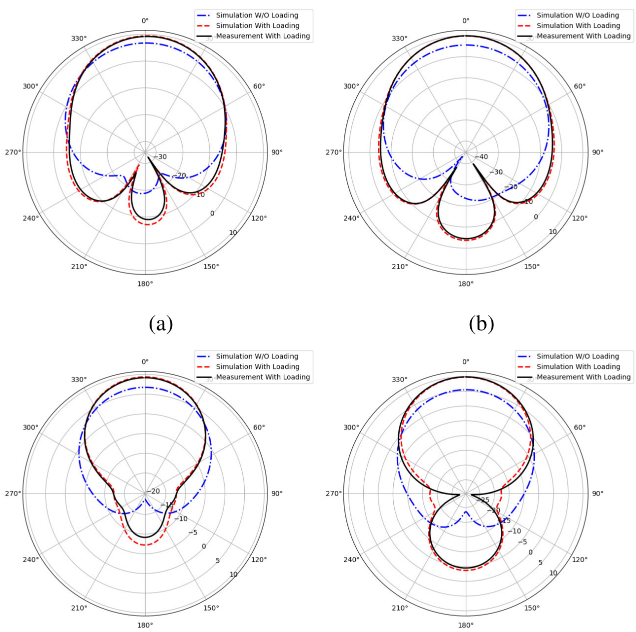

(a) (b)

(c) (d)

FIGURE 25. **Measured and simulated Radiation pattern of the proposed array with and without the proposed loading structure across E-plane at (a) 5.8 GHz, (b) 6 GHz, and across H-plane at (c) 5.8 GHz and (d) 6 GHz.**

not compromise impedance matching. This demonstrates that the proposed structure achieves strong mutual coupling suppression while preserving element matching performance.

D. RADIATION CHARACTERISTICS

The simulated radiation patterns of the array with and without the decoupling structure along with the measured results of the loaded array are shown in Fig. 25 at 5.8 GHz and 6 GHz for both E- and H-planes. It can be observed that the overall radiation characteristics remain directed toward the broadside direction. This indicates that the introduction of the decoupling mechanism does not alter the main radiation direction of the antenna array, which is an important consideration in array design. The measured realized gains are 9.21 dBi and 9.86 dBi at 5.8 GHz and 6 GHz, respectively. These results correspond to gain improvements of 2.45 dB and 4.34 dB at the lower and upper edges of the operating frequency band, respectively, highlighting the effectiveness of the proposed decoupling structure in enhancing the realized gain of the antenna array. It is worth noting that, the gain enhancement produced by the proposed decoupling structure is frequency dependent due to the resonant nature of the employed coupling suppression mechanisms. As the electromagnetic interaction between the decoupling structure and the antenna array varies across the operating band, the degree of mutual coupling reduction and radiation efficiency improvement also changes. Consequently, larger gain enhancement is observed at frequencies where the decoupling mechanism operates closer to its optimum condition.

Compared to the simulated results, the measured realized gain exhibits a reduction of approximately 0.4 dB, which can mainly be attributed to the insertion loss introduced by the RF connectors used during measurement. Aside from this minor discrepancy, the simulated and measured results show good agreement, further confirming the validity of the proposed design.

The realized gain remains stable across the operating band, confirming that the proposed decoupling approach does not introduce significant radiation efficiency degradation. The absence of noticeable pattern distortion further validates that the isolation improvement is achieved without compromising radiation integrity, which is critical for ultra-compact arrays.

TABLE 2. **Performance comparison with reported loaded decoupling techniques.**

Ref.	Array Type	Array Size (λ_0)	Edge-to-Edge Spacing (λ_0)	Isolation (dB)
Ref. [47]	2×2 Patch	$1.01\times1.01\times0.013$	0.2	>30
Ref. [39]	2×2 Patch	$2.1\times1.92\times0.29$	(0.11,0.28)	>25
This Work	**2×2 Patch**	**0.638×0.638×0.193**	**0.038**	**>20**

E. BENCHMARKING AND COMPARATIVE ANALYSIS

To further demonstrate the advantages of the proposed design, a comparison with recently reported decoupling techniques is provided in Table 2. The comparison includes array configuration, array size, edge-to-edge spacing, and achieved isolation.

Compared with existing works, the proposed array operates at a significantly smaller inter-element spacing while achieving competitive isolation performance.

IV. CONCLUSION AND FUTURE WORKS

This paper presented the design, optimization, and experimental validation of an ultra-compact 2×2 antenna array with a center-to-center spacing smaller than 0.3λ. In such densely packed configurations, strong multidirectional mutual coupling becomes unavoidable and significantly degrades impedance matching, isolation, and radiation performance. The primary objective of this work was therefore to achieve an isolation level better than -20 dB within the operating frequency range of 5.8–6 GHz, while preserving gain and maintaining a low-profile, without any complexity in fabrication.

To address the inherently two-dimensional coupling behavior of the planar array, a comprehensive decoupling strategy was developed. The proposed solution integrates I-shaped metallic strips to enhance coupling-path cancellation, a dumbbell-shaped DGS to suppress ground-plane current propagation, and a dielectric perturbation technique to reduce substrate-mediated coupling. The combined effect of these mechanisms enables effective suppression of mutual coupling in both principal planar directions without relying on multilayer metasurface assemblies.

A detailed parametric study was conducted to investigate the influence of the key geometrical parameters on isolation and impedance matching. The results demonstrated that the vertical stem length primarily controls the resonant behavior of the decoupling element, while the horizontal arm dimensions regulate the interaction between adjacent strips. The DGS dimensions and substrate slot length were shown to significantly affect inter-row coupling by interrupting surface currents and redistributing the electromagnetic fields. The antenna-to-decoupling spacing was also optimized to achieve strong isolation while maintaining a compact profile. To systematically determine the optimal parameter set, a GA optimization was employed, enabling efficient exploration of the design space.

Both simulated and measured results confirm that the proposed structure successfully reduces the transmission coefficients between array elements to below -20 dB across the target frequency band. Importantly, this isolation enhancement is achieved without significant degradation of impedance matching and realized gain. The measured radiation patterns further demonstrate that the decoupling structure does not distort the radiation characteristics, validating that coupling suppression is accomplished without compromising radiation integrity. Compared to previously reported works, the proposed design achieves competitive isolation at a smaller inter-element spacing while maintaining structural simplicity and manufacturability.

In summary, this work provides a practical and scalable decoupling methodology for ultra-compact planar arrays, where multidirectional coupling suppression, gain preservation, and low-profile implementation are simultaneously required.

Future work may extend the proposed concept to larger planar arrays, wide-angle beam-scanning configurations, and higher-frequency systems, including Ka-band and FR2 applications, to evaluate its performance under active excitation conditions and different electromagnetic environments. In addition, advanced computational techniques, such as machine learning and artificial intelligence methods, may be employed to further enhance the efficiency of the optimization process and accelerate electromagnetic performance evaluation. The integration of the proposed decoupling mechanism into circularly polarized and dual-polarized array architectures also represents a promising direction for advanced communication systems.

REFERENCES

[1] M. Feng, S. Mao, and T. Jiang, "Base station ON–OFF switching in 5G wireless networks: Approaches and challenges," *IEEE Wireless Commun.*, vol. 24, no. 4, pp. 46–54, Aug. 2017.

[2] E. G. Larsson, O. Edfors, F. Tufvesson, and T. L. Marzetta, "Massive MIMO for next generation wireless systems," *IEEE Commun. Mag.*, vol. 52, no. 2, pp. 186–195, Feb. 2014.

[3] Y.-H. Nam, B. L. Ng, K. Sayana, Y. Li, J. Zhang, Y. Kim, and J. Lee, "Full-dimension MIMO (FD-MIMO) for next generation cellular technology," *IEEE Commun. Mag.*, vol. 51, no. 6, pp. 172–179, Jun. 2013.

[4] M. Jiang and L. Hanzo, "Multiuser MIMO-OFDM for next-generation wireless systems," *Proc. IEEE*, vol. 95, no. 7, pp. 1430–1469, Jul. 2007.

[5] R. Becher, M. Dillinger, M. Haardt, and W. Mohr, "Broadband wireless access and future communication networks," *Proc. IEEE*, vol. 89, no. 1, pp. 58–75, Jan. 2001.

[6] H. Zhang, Z. Wang, J. Yu, and J. Huang, "A compact MIMO antenna for wireless communication," *IEEE Antennas Propag. Mag.*, vol. 50, no. 6, pp. 104–107, Jun. 2008.

[7] H. T. Hui, "Decoupling methods for the mutual coupling effect in antenna arrays: A review," *Recent Patents Eng.*, vol. 1, no. 2, pp. 187–193, Jun. 2007.

[8] Y. Hu, Y. M. Pan, and M. Di Yang, "Circularly polarized MIMO dielectric resonator antenna with reduced mutual coupling," *IEEE Trans. Antennas Propag.*, vol. 69, no. 7, pp. 3811–3820, Jul. 2021.

[9] H. Singh, H. L. Sneha, and R. M. Jha, "Mutual coupling in phased arrays: A review," *Int. J. Antennas Propag.*, vol. 2013, no. 1, 2013, Art. no. 348123.

[10] V. Agrawal and Y. Lo, "Mutual coupling in phased arrays of randomly spaced antennas," *IEEE Trans. Antennas Propag.*, vol. AP-20, no. 3, pp. 288–295, May 1972.

[11] R. Liu, X. An, H. Zheng, M. Wang, Z. Gao, and E. Li, "Neutralization line decoupling tri-band multiple-input multiple-output antenna design," *IEEE Access*, vol. 8, pp. 27018–27026, 2020.

[12] M. Li, L. Jiang, and K. L. Yeung, "A general and systematic method to design neutralization lines for isolation enhancement in MIMO antenna arrays," *IEEE Trans. Veh. Technol.*, vol. 69, no. 6, pp. 6242–6253, Jun. 2020.

[13] S. Zhang and G. F. Pedersen, "Mutual coupling reduction for UWB MIMO antennas with a wideband neutralization line," *IEEE Antennas Wireless Propag. Lett.*, vol. 15, pp. 166–169, 2016.

[14] H. Meng and K.-L. Wu, "An LC decoupling network for two antennas working at low frequencies," *IEEE Trans. Microw. Theory Techn.*, vol. 65, no. 7, pp. 2321–2329, Jul. 2017.

[15] H. V. Singh, D. V. S. Prasad, and S. Tripathi, "Dual-band MIMO antenna decoupling using vias based multipath decoupling circuit," *Microw. Opt. Technol. Lett.*, vol. 64, no. 4, pp. 770–777, Apr. 2022.

[16] L. Sun, Y. Li, and Z. Zhang, "Decoupling between extremely closely spaced patch antennas by mode cancellation method," *IEEE Trans. Antennas Propag.*, vol. 69, no. 6, pp. 3074–3083, Jun. 2021.

[17] W. Yang, L. Chen, S. Pan, W. Che, and Q. Xue, "Novel decoupling method based on coupling energy cancellation and its application in 5G dual-polarized high-isolation antenna array," *IEEE Trans. Antennas Propag.*, vol. 70, no. 4, pp. 2686–2697, Apr. 2022.

[18] M. Li, L. Jiang, and K. L. Yeung, "Novel and efficient parasitic decoupling network for closely coupled antennas," *IEEE Trans. Antennas Propag.*, vol. 67, no. 6, pp. 3574–3585, Jun. 2019.

[19] M. Li and S. Cheung, "A novel calculation-based parasitic decoupling technique for increasing isolation in multiple-element MIMO antenna arrays," *IEEE Trans. Veh. Technol.*, vol. 70, no. 1, pp. 446–458, Jan. 2021.

[20] Q. X. Lai, Z. L. Hu, and Y. M. Pan, "A simple decoupling method for wideband millimeter-wave MIMO magnetoelectric dipole antenna array using parasitic stubs," *IEEE Trans. Antennas Propag.*, vol. 72, no. 10, pp. 7470–7479, Oct. 2024.

[21] Y.-M. Zhang and S. Zhang, "A side-loaded-metal decoupling method for $2 \times N$ patch antenna arrays," *IEEE Antennas Wireless Propag. Lett.*, vol. 20, no. 5, pp. 668–672, May 2021.

[22] B. K. Lau and J. B. Andersen, "Simple and efficient decoupling of compact arrays with parasitic scatterers," *IEEE Trans. Antennas Propag.*, vol. 60, no. 2, pp. 464–472, Feb. 2012.

[23] A. I. Afifi, A. S. A. El-Hameed, A. Allam, S. M. Ahmed, and A. B. Abdel-Rahman, "Dual port MIMO antenna with low mutual coupling based on asymmetric EBG decoupling structure," in *Proc. 15th Eur. Conf. Antennas Propag. (EuCAP)*, Mar. 2021, pp. 1–5.

[24] J.-Y. Lee, S.-H. Kim, and J.-H. Jang, "Reduction of mutual coupling in planar multiple antenna by using 1-D EBG and SRR structures," *IEEE Trans. Antennas Propag.*, vol. 63, no. 9, pp. 4194–4198, Sep. 2015.
[25] A. Khan, S. Bashir, S. Ghafoor, and K. K. Qureshi, "Mutual coupling reduction using ground stub and EBG in a compact wideband MIMO-antenna," *IEEE Access*, vol. 9, pp. 40972–40979, 2021.
[26] M. I. Ahmed, A. Sebak, E. A. Abdallah, and H. Elhennawy, "Mutual coupling reduction using defected ground structure (DGS) for array applications," in *Proc. 15 Int. Symp. Antenna Technol. Appl. Electromagn.*, Jun. 2012, pp. 1–5.
[27] D. Gao, Z.-X. Cao, S.-D. Fu, X. Quan, and P. Chen, "A novel slot-array defected ground structure for decoupling microstrip antenna array," *IEEE Trans. Antennas Propag.*, vol. 68, no. 10, pp. 7027–7038, Oct. 2020.
[28] B. Qian, X. Chen, and A. A. Kishk, "Decoupling of microstrip antennas with defected ground structure using the common/differential mode theory," *IEEE Antennas Wireless Propag. Lett.*, vol. 20, no. 5, pp. 828–832, May 2021.
[29] M. Akbari, H. A. Ghalyon, M. Farahani, A.-R. Sebak, and T. A. Denidni, "Spatially decoupling of CP antennas based on FSS for 30-GHz MIMO systems," *IEEE Access*, vol. 5, pp. 6527–6537, 2017.
[30] P. Mondal, D. Dhara, and A. R. Harish, "A partially reflective FSS-based superstrate as a decoupling structure for reducing the mutual coupling of circularly polarized antennas," *IEEE Trans. Antennas Propag.*, vol. 72, no. 4, pp. 3652–3661, Apr. 2024.
[31] F. Merzaki, P. Besnier, M. Himdi, X. Castel, M. Sergolle, T. Levavasseur, and P. Caldamone, "A compact double-sided FSS absorbing wall for decoupling 5G antenna arrays," *IEEE Trans. Electromagn. Compat.*, vol. 64, no. 2, pp. 303–314, Apr. 2022.
[32] Y. Zhu, Y. Chen, and S. Yang, "Decoupling and low-profile design of dual-band dual-polarized base station antennas using frequency-selective surface," *IEEE Trans. Antennas Propag.*, vol. 67, no. 8, pp. 5272–5281, Aug. 2019.
[33] W. Zhou, J. Qi, Y. Li, and T. Jiang, "A low coupling broadband MIMO antenna for 5G using meta-surface decoupling structure," in *Proc. IEEE Int. Symp. Antennas Propag. USNC-URSI Radio Sci. Meeting (AP-S/URSI)*, Jul. 2022, pp. 1784–1785.
[34] Z. Wang, L. Zhao, Y. Cai, S. Zheng, and Y. Yin, "A meta-surface antenna array decoupling (MAAD) method for mutual coupling reduction in a MIMO antenna system," *Sci. Rep.*, vol. 8, no. 1, p. 3152, Feb. 2018.
[35] F. Liu, J. Guo, L. Zhao, G.-L. Huang, Y. Li, and Y. Yin, "Dual-band metasurface-based decoupling method for two closely packed dual-band antennas," *IEEE Trans. Antennas Propag.*, vol. 68, no. 1, pp. 552–557, Jan. 2020.
[36] Z. Wang, C. Li, Q. Wu, and Y. Yin, "A metasurface-based low-profile array decoupling technology to enhance isolation in MIMO antenna systems," *IEEE Access*, vol. 8, pp. 125565–125575, 2020.
[37] I. Khan, X. Qi, Y. Shao, K. Zhang, C. Song, M. M. Kamal, and Q. Wu, "Hybrid technique-based circularly polarized MIMO antenna with low mutual coupling for millimeter-wave communications," *Opt. Exp.*, vol. 33, no. 8, pp. 17782–17801, 2025.
[38] D.-L. Wu, W. H. Guo, W. J. Zhu, F. Jiang, and L. H. Ye, "Broadband hybrid decoupling method for a dual-polarized antenna with high isolation," *IEEE Antennas Wireless Propag. Lett.*, vol. 23, no. 7, pp. 2165–2169, Jul. 2024.
[39] K.-L. Wu, C. Wei, X. Mei, and Z.-Y. Zhang, "Array-antenna decoupling surface," *IEEE Trans. Antennas Propag.*, vol. 65, no. 12, pp. 6728–6738, Dec. 2017.
[40] Z. Wei, Z. Zhou, P. Wang, J. Ren, Y. Yin, G. F. Pedersen, and M. Shen, "Fully automated design method based on reinforcement learning and surrogate modeling for antenna array decoupling," *IEEE Trans. Antennas Propag.*, vol. 71, no. 1, pp. 660–671, Jan. 2023.
[41] A. Ebrahimi, T. Baum, and K. Ghorbani, "Differential bandpass filters based on dumbbell-shaped defected ground resonators," *IEEE Microw. Wireless Compon. Lett.*, vol. 28, no. 2, pp. 129–131, Feb. 2018.
[42] J.-Y. Hou, H. Zhou, L. Peng, and F.-Y. Sun, "A broadband absorptive common-mode filter based on SRR dumbbell-shaped DGS and inter-digital capacitor," *IEEE Trans. Electromagn. Compat.*, vol. 68, no. 3, pp. 613–621, Jun. 2026.
[43] Z. Gan, Z.-H. Tu, Z.-M. Xie, Q.-X. Chu, and Y. Yao, "Compact wideband circularly polarized microstrip antenna array for 45 GHz application," *IEEE Trans. Antennas Propag.*, vol. 66, no. 11, pp. 6388–6392, Nov. 2018.
[44] Y. Xu, S. Gong, and T. Hong, "Circularly polarized slot microstrip antenna for harmonic suppression," *IEEE Antennas Wireless Propag. Lett.*, vol. 12, pp. 472–475, 2013.
[45] Y. Hu, J. Sui, and X. Zhu, "A self-decoupled microstrip antenna via inhomogeneous substrate manipulation," *IEEE Trans. Antennas Propag.*, vol. 74, no. 6, pp. 5122–5133, Jun. 2026.
[46] Y. Aslan and A. Yarovoy, "Reduction of mutual coupling between closely spaced patch antennas using dielectric stratification technique," in *Proc. 47th Eur. Microw. Conf. (EuMC)*, Oct. 2017, pp. 248–251.
[47] D. Gao, Z. Cao, X. Quan, M. Sun, S. Fu, and P. Chen, "A low-profile decoupling slot-strip array for 2 × 2 microstrip antenna," *IEEE Access*, vol. 8, pp. 113532–113542, 2020.

SINA HASIBI TAHERI received the B.S. and M.S. degrees in electrical engineering from the Department of Electrical Engineering (EE), Amirkabir University of Technology, Iran, in 2009 and 2011, respectively. He is currently pursuing the Ph.D. degree with the School of Engineering, Macquarie University, Sydney, NSW, Australia. He was a Researcher with the KNTU Telecommunication Research Center, from 2011 to 2023. His research interests include phased arrays, numerical techniques in electromagnetics, and machine learning and AI applications in telecommunication.

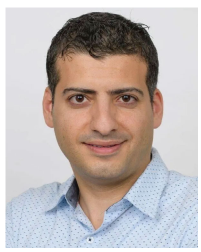

ALI LALBAKHSH (Senior Member, IEEE) received the B.S. and M.S. degrees in electronic and telecommunication engineering, in 2008 and 2011, respectively, and the H.D. and Ph.D. degrees in electronics engineering from Macquarie University, Australia, in 2015 and 2020, respectively. He is currently a Lecturer at the UNSW College, Sydney, Australia. He has published over 120 peer-reviewed journals and conference papers. His research interests include satellite communication, high-gain antennas, evolutionary optimization methods, and passive microwave components. He received several prestigious awards, including the International Research Training Program Scholarship (iRTP) for the MRes, the International Macquarie University Research Excellence Scholarship (iMQRES) for the Ph.D. degree, the Commonwealth Scientific and Industrial Research Organization (CSIRO) grants on Astronomy and Space Exploration, the Macquarie University Postgraduate Research Fund (PGRF), and the WiMed Travel Support Grants. He was a recipient of the 2016 ICEAA-IEEE APWC Cash Prize and the Macquarie University Deputy Vice-Chancellor Commendation, in 2017. He is also a Researcher in the IEEE Region 10 (Asia–Pacific) and has received the Most Prestigious Best Paper Contest of the IEEE Region 10, for many times. He received the third prize, the first prize, and the second prize from the international competition, in 2016, 2018, and 2019, respectively. He was highly commended as a Finalist and the Winner of the Excellence in Higher Degree Research Award in Science, Technology, Engineering, Mathematics and Medicine (STEMM), Macquarie University, in 2019 and 2020, respectively. In 2020, he was announced as an Outstanding Reviewer of IEEE Transactions on Antennas and Propagation; and received the Research Excellence Award of the Faculty of Science and Engineering, Macquarie University. He serves as an Associate Editor for *International Journal of Electronics and Communications and Electronics* (MDPI).

NABEEL ZAHUR received the B.S. degree in electrical and electronics engineering (EEE) from the University of Sharjah, Sharjah, United Arab Emirates, in 2018, and the M.S. degree in electronics engineering from Macquarie University, Sydney, NSW, Australia, in 2020. He is currently an Electronics Engineer based in NSW, Australia. His research and professional interests include RF systems design, high-speed PCB layout, and signal integrity.

SLAWOMIR KOZIEL (Fellow, IEEE) received the M.Sc. and Ph.D. degrees in electronic engineering from Gdańsk University of Technology, Poland, in 1995 and 2000, respectively, and the M.Sc. degree in theoretical physics and the M.Sc. and Ph.D. degrees in mathematics from the University of Gdańsk, Poland, in 2000, 2002, and 2003, respectively. He is currently a Professor with the Department of Engineering, Reykjavik University, Iceland. His current research interests include the CAD and modeling of microwave and antenna structures, simulation-driven design, surrogate-based optimization, space mapping, circuit theory, analog signal processing, evolutionary computation, and numerical analysis.

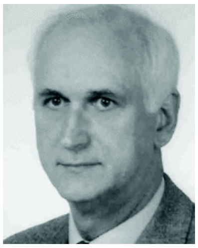

STANISLAW SZCZEPANSKI (Member, IEEE) received the M.Sc. and Ph.D. degrees in electronic engineering from Gdańsk University of Technology, Gdańsk, Poland, in 1975 and 1986, respectively. In 1986, he joined the Institut National Polytechnique de Toulouse (INPT), Toulouse, France, as a Visiting Research Associate. From 1990 to 1991, he was with the Department of Electrical Engineering, Portland State University, Portland, OR, USA, on a Kosciuszko Foundation Fellowship. From August 1998 to September 1998, he was a Visiting Professor with the Faculty of Engineering and Information Sciences, University of Hertfordshire, Hatfield, U.K. He is currently a Professor with the Department of Microelectronic Systems, Faculty of Electronics, Telecommunications and Informatics, Gdańsk University of Technology. He has published more than 160 articles and holds three patents. His research interests include circuit theory, fully integrated analog filters, high-frequency transconductance amplifiers, analog integrated circuit design, and analog signal processing.

AMIRHASSAN ZAREANBORJI (Member, IEEE) received the Ph.D. degree in electrical engineering—telecommunication from UNSW, Sydney, Australia. He is currently a Lecturer at the UNSW College. He has extensive industry experience in telecommunications network planning and design. His research interests include telecommunication, optics, photonic, and sustainable engineering solutions.